Available online at www.sciencedirect.com
SCIENCE DIRECT®
Journal of Colloid and Interface Science 272 (2004) 330–339
JOURNAL OF Colloid and Interface Science
www.elsevier.com/locate/jcis

Rigorous calculations of linearized Poisson–Boltzmann interaction between dissimilar spherical colloids and osmotic pressure in concentrated dispersions

Myung-Suk Chun [a,*] and W. Richard Bowen [b]

[a] *Complex Fluids and Membrane Team, Korea Institute of Science and Technology (KIST), P.O. Box 131, Cheongryang, Seoul 130-650, South Korea*
[b] *Centre for Complex Fluids Processing, Department of Chemical and Biological Process Engineering, University of Wales Swansea, Singleton Park, Swansea SA2 8PP, UK*

Received 16 June 2003; accepted 2 December 2003

Abstract

We present computational results on the static properties of concentrated dispersions of bidisperse colloids. The long-range electrostatic interactions between dissimilar spherical colloids are determined using the singularity method, which provides rigorous solutions to the linearized electrostatic field. The NVT Monte Carlo simulation is applied to the bulk suspension to obtain the radial distribution function for the concentrated system. The increasing trend of osmotic pressure with increasing total particle concentration is reduced as the concentration ratio between large and small particles is increased. The increase of electrostatic interaction between similarly charged particles caused by the Debye screening effect provides an increase in the osmotic pressure. From the estimation of total structure factor, we observe the strong correlations developed between dissimilar spheres, and the small spheres are expected to tend to fit into the spaces between the larger ones. As the particle concentration increases at a given ionic strength, the magnitude of the first peak in structure factors increases and also moves to higher wavenumber values.

Keywords: Bidisperse colloid; Poisson–Boltzmann equation; Electrostatic interaction; Radial distribution function; Osmotic pressure; Structure factor

1. Introduction

Osmotic pressure of a colloidal suspension provides a quantification of the interactions between colloids in a concentrated system. Since the analysis of multiparticle interactions is not succinct, most of the relevant studies have been confined to dilute systems. Osmotic pressure is therefore of substantial fundamental and practical significance in the processing of complex fluids, such as nanoparticle dispersion, membrane filtration, and particulate processing.

It was reported that the osmotic pressure for a wide concentration range of proteins or other electrostatically stabilized colloids may be calculated accurately via use of extended Derjaguin–Landau–Verwey–Overbeek (DLVO) theory [1–3]. Bowen et al. [3] also examined the application of osmotic pressure in the calculation of the gradient diffusion coefficient from the general Stokes–Einstein equation, where the electric field is governed by the nonlinear Poisson–Boltzmann (P–B) equation. The physicochemical effects of both the solution ionic strength and the pH were considered; their model takes into account multiparticle electrostatic interactions, London–van der Waals forces, and the entropic pressure. Later, they compared the particle concentration dependency upon the thermodynamic coefficients determined by dilute limit calculation, hypernetted-chain closure, radial distribution method, and cell model calculation [4].

The monodisperse colloidal suspension can be a well-defined model for theoretical investigations; however, this ideal system is hardly found in practical situations. The distribution of particle size explicitly affects the microstructure of colloidal dispersions, and this behavior becomes more significant as the particle concentration increases. The difficulty of the relevant analytical solution will be dramatically increased, even though it is a bidisperse problem.

The microstructural properties of a colloidal dispersion can be studied by Monte Carlo simulations, and they pro-

* Corresponding author.
E-mail address: mschun@kist.re.kr (M.-S. Chun).

0021-9797/$ – see front matter
doi:10.1016/j.jcis.2003.12.005

vide an exact answer for the given model within statistical uncertainty. Chun et al. [5] predicted both the thermodynamic coefficient and the gradient diffusion coefficient with variations of particle concentration as well as ionic strength, with which the profile of the concentration polarization layer during the membrane filtration of latex suspensions was obtained. In their investigation, the radial distribution function was successfully determined by employing the Monte Carlo simulation for charged colloids with higher concentrations (i.e., up to 50 vol%). The rigorous calculation of the long-range electrostatic interaction with the linearized P–B field was performed using a singularity method, which was proposed by Phillips [6] as a useful scheme for multisphere systems. This method is similar to that described by Dabros [7] for use in low-Reynolds-number hydrodynamics problem.

Carnie et al. [8] derived the electric double-layer interaction energy between dissimilar spherical colloids based on a two-center expansion in terms of spherical harmonics for a linearized P–B field. The calculation of electrostatic energy of interaction between two dissimilar spheres was also conducted by Ohshima [9,10] by employing the method of reflection in boundary value problems on the basis of the linearized P–B equation without recourse to numerical methods. We applied the singularity method again in this study, in which the electrostatic potential in the liquid can be represented as a sum of contributions from point charges located inside the spheres, if the dielectric constant of a solid particle is assumed to be small relative to that of the surrounding liquid. These point charges are expressed by the fundamental singular solution to the linearized P–B equation. The strengths of the singularities are chosen to provide the best possible agreement with the prescribed boundary conditions.

In this study, we first calculate the long-range interaction between dissimilar spherical colloids and then use the Metropolis Monte Carlo method to obtain the radial distribution function. Our simulation results for uncharged systems are compared with results from theoretical work obtained using an integral equation method. Although the colloidal interactions originate from various forces, the long-range force due to the electrostatic repulsion is considered. The osmotic pressure is estimated for suspensions of both uncharged and charged cases, from which the concentration dependence of the osmotic pressure is investigated as a function of the volume fraction ratio of large to small spheres. Utilizing the radial distribution function, the static structure factor is estimated and we discuss the encountered phenomena.

2. Long-range electrostatic interaction between dissimilar spheres

The singularity method applied here has been proved to overcome the restrictions of the Derjaguin approximation as well as the linear superposition approximation. Let us examine a problem of N identical charged spheres interacting in solution. The electrostatic potential is governed by a linearized P–B equation,

$$\nabla^2\psi = (\kappa a)^2\psi, \tag{1}$$

where the electrostatic potential ψ is normalized by a characteristic surface potential, and the inverse Debye length (or double layer thickness) κ defined as $\sqrt{(e^2 N_A \sum_i c_i^0 Z_i^2)/\varepsilon kT}$ is made dimensionless by the sphere radius a. Note that e is the elementary Coulombic charge, N_A the Avogadro number, ε a dielectric constant, kT the Boltzmann thermal energy, c_i^0 the concentration of ion species i far from the sphere (in moles per unit volume), and Z_i its valence. We consider here the condition of overall electroneutrality in an equilibrium solution. For aqueous solutions of monovalent electrolytes at 25 °C, the Debye length κ^{-1} (nm) is given by (solution ionic strength (mol))$^{-1/2}$/3.278.

Suitable boundary conditions known as constant charge, constant potential, and the linearized charge regulation can commonly be used in obtaining solutions to Eq. (1). Among them, we consider the sphere surfaces S_A having a constant surface-charge density σ, leading to the constant charge boundary condition

$$\mathbf{n}\cdot\nabla\psi = \sigma \quad \text{on } S_A, \tag{2}$$

where $\mathbf{n}$ is a unit normal vector pointing into the sphere. The singular solution to Eq. (1) for a point charge at the origin has the form ($\psi = q\exp(-\kappa a r)/r$) with an unknown constant q and the distance r from the origin normalized by the sphere radius. For an isolated sphere suspended in an unbounded solution, the value of q can be determined from the boundary condition.

We consider the bidisperse colloidal suspensions of charged spheres with radii a_l and a_s as shown in Fig. 1, where the subscripts refer to the large and small ones, respectively. Both spheres, when they are isolated and not interacting with each other, have surface potentials ψ_s of 1 equal to $kT/e = 25.69$ mV. The principal calculation step is similar to a problem of equal-sized spheres. However, the location of the surface points and the singular points inside the spheres should be newly developed according to the sphere radii ratio a_l/a_s.

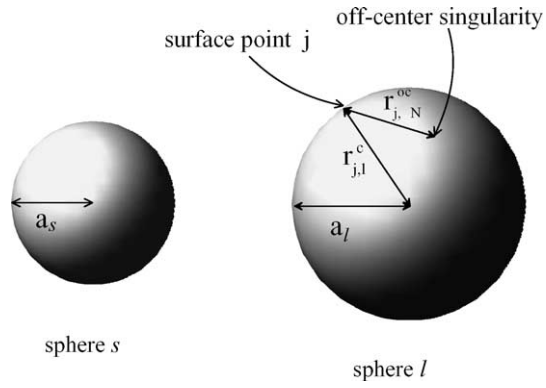

Fig. 1. Interaction between two charged spherical colloids l and s of radii a_l and a_s.

The total surface charge outside the spheres is expressed as the addition of the sum of the known contribution of singularities at the sphere centers $\mathbf{n}\cdot\nabla\psi_i^c$ and the sum of the corresponding contribution of off-center singularities $\mathbf{n}\cdot\nabla\psi_i^{\mathrm{oc}}$. There are α off-center singularities for each of the N spheres. Considering the surface charge density σ at a surface point $\mathbf{x}_j$, the following can be written:

$$\sum_{i=1}^{\alpha N}\mathbf{n}\cdot\nabla\psi_i^{\mathrm{oc}}(\mathbf{x}_j)=\sigma(\mathbf{x}_j)-\sum_{i=1}^{N}\mathbf{n}\cdot\nabla\psi_i^{c}(\mathbf{x}_j)\quad\text{for } j=1 \text{ to } M. \tag{3}$$

Equation (3) provides M linear equations for the αN unknown singularity strengths q_i^{oc}, where M is the total number of surface points of two dissimilar spheres (i.e., $N=2$) and a_l takes the basis of the characteristic length for the sphere radius. Thus, the following matrix is formulated,

$$\begin{bmatrix} d_{1,1} & \cdots & d_{1,\alpha} & \cdots & d_{1,2\alpha} \\ \vdots & & \vdots & & \vdots \\ d_{M/2,1} & \cdots & d_{M/2,\alpha} & \cdots & d_{M/2,2\alpha} \\ \vdots & & \vdots & & \vdots \\ d_{M,1} & \cdots & d_{M,\alpha} & \cdots & d_{M,2\alpha} \end{bmatrix}\begin{bmatrix} q_1^{\mathrm{oc}} \\ \vdots \\ q_\alpha^{\mathrm{oc}} \\ \vdots \\ q_{2\alpha}^{\mathrm{oc}} \end{bmatrix} = \begin{bmatrix} b_1 \\ \vdots \\ b_{M/2} \\ \vdots \\ b_M \end{bmatrix}, \tag{4}$$

where

$$d_{j,k}=n\cdot\nabla\left(\frac{\exp(-\kappa a_l r_{j,k}^{\mathrm{oc}})}{r_{j,k}^{\mathrm{oc}}}\right)\quad\text{for } j=1 \text{ to } M,\ k=1 \text{ to } 2\alpha, \tag{5a}$$

$$b_j=\sigma(\mathbf{x}_j)-\mathbf{n}\cdot\nabla\left(q_1^c\frac{\exp(-\kappa a_l r_{j,1}^c)}{r_{j,1}^c}+q_2^c\frac{\exp(-\kappa a_l r_{j,2}^c)}{r_{j,2}^c}\right). \tag{5b}$$

From Eq. (4), the value of q_i^{oc} is found by a least-squares routine that minimizes the sum of squared residuals at the surface points. For surface potential ψ_s, the dimensionless surface charge densities of each sphere are expressed as

$$\sigma_l=\psi_{s,l}(1+\kappa a_l)\quad\text{for large sphere,} \tag{6a}$$

$$\sigma_s=\psi_{s,s}(1+\kappa a_s)\left(\frac{a_l}{a_s}\right)\quad\text{for small sphere.} \tag{6b}$$

The force on a charged sphere interacting with other charged spheres is calculated by accounting for the spherical coordinates. The strength of each point singularity is determined by satisfying the boundary conditions. Once the solution for the potential is obtained, the force vector $\mathbf{F}$ is calculated from the surface integration of normal component of Maxwell stress tensor $\mathbf{T}$, as follows:

$$\mathbf{F}=\int_{S_A}\mathbf{T}\cdot\mathbf{n}\,dS_A. \tag{7}$$

The Maxwell stress tensor is given by

$$\mathbf{T}=\left(\widetilde{\Pi}+\varepsilon\frac{\mathbf{E}\cdot\mathbf{E}}{2}\right)\mathbf{I}-\varepsilon\mathbf{E}\mathbf{E}, \tag{8}$$

where $\mathbf{I}$ is the identity tensor and $\mathbf{E}$ $(=-\nabla\psi)$ denotes the electric field vector. The electrostatic potential is related to the difference in the local osmotic pressure $\widetilde{\Pi}$ from the bulk solution given by $\varepsilon\kappa^2\psi^2/2$ [11,12]. Then the electrostatic interaction energy profile between pairs of spheres with separation distance between two spheres s' can be obtained by integrating the force acting on the sphere,

$$E_{\mathrm{EL}}(s')=\int_{-\infty}^{s'}F_x\,dx=\int_{-\infty}^{s'}\left[\mathbf{e}_x\cdot\int_{S_A}\mathbf{T}\cdot\mathbf{n}\,dS_A\right]dx=\int_{S_A}[\cos\theta T_{rr}-\sin\theta T_{\theta r}]r^2\sin\theta\,d\theta\,d\varphi, \tag{9}$$

where dS_A is defined in spherical coordinates (r,θ,φ). For the center-to-center separation distance s, the surface-to-surface distance s' corresponds to $s-(a_l+a_s)$ for dissimilar spheres, whereas s' equals $s-2a_l$ for two large spheres and $s-2a_s$ for two small spheres.

Although this study does not consider the van der Waals dispersion forces between the atoms in two dissimilar approaching spheres, they are additive and act over a relatively long range. The Hamaker constant for a given material is necessary to obtain the attractive interaction energy.

3. Static properties of concentrated dispersions

3.1. Osmotic pressure from Monte Carlo simulations

The osmotic pressure Π is related to the thermodynamic coefficient S as [3,4]

$$S(C)=\left[\frac{\partial\Pi(C)}{\partial C}\frac{4\pi a^3}{3kT}\right]^{-1}, \tag{10}$$

where C is the particle concentration in terms of volume fraction. Note that the coefficient $S(C)$ coincides with the structure factor of the suspension at the zero scattering vector. The osmotic pressure is expressed in the form of a virial equation as [1]

$$\Pi(C)=\frac{3kT}{4\pi a^3}C\left(1+A_2C+A_3C^2+\cdots\right), \tag{11}$$

where A_2 and A_3 are osmotic virial coefficients. It is possible to derive the analytical solution in power series of the particle concentration as

$$S(C)=1-2A_2C+\left(2A_2^2-3A_3\right)C^2+O\left(C^3\right). \tag{12}$$

Here, A_2 is represented by

$$A_2 = \frac{3}{2a^3}\int_0^\infty \big[1 - g(s)\big]s^2\,ds, \tag{13}$$

where $g(s)$ is the radial distribution function.

Many investigations exist for the analysis on the radial distribution function. For a dilute suspension, the radial distribution function is simply given by the Boltzmann distribution [5]

$$g(s) = \exp\left(-\frac{E(s)}{kT}\right). \tag{14}$$

Here, $E(s)$ is the pairwise interaction energy of repulsive potentials, which is obtained from Eq. (9). Once the effect of long-range colloidal interactions is absent in the concentrated suspension, the radial distribution function can be determined by integral equations, perturbation methods, and Monte Carlo simulations [13]. Among these, the Monte Carlo simulations enable the prediction of the charged suspension over the full range of particle concentrations.

3.2. Static structure factor

The important microstructural information can be acquired by means of the structure factor, which gives all length scale data [14,15]. Considering the phase difference between the scattered beams from two particles at $\mathbf{r}_i^l$ and $\mathbf{r}_j^s$, the scattering vector $\mathbf{Q}$ has a magnitude $(4\pi/\lambda)\sin(\theta/2)$, where λ is the wavelength in the dispersion medium and θ the scattering angle. The static structure factor $S_f(\mathbf{Q})$ for a bidisperse suspension can be directly obtained from the radial distribution function, defined as

$$S_f(\mathbf{Q}) = \frac{1}{N}\sum_{i=1}^{N_l}\sum_{j=1}^{N_s}\big\langle\exp\big(i\mathbf{Q}\cdot\big(\mathbf{r}_i^l - \mathbf{r}_j^s\big)\big)\big\rangle, \tag{15}$$

where $N\ (= N_l + N_s)$ denotes the number of spheres and the brackets mean an ensemble average. After spherical averaging, Eq. (15) yields

$$S_f(Q) = \delta_{ls} + \frac{4\pi\sqrt{n_l n_s}}{Q}\int_0^\infty \big[g(s) - 1\big]s\sin Qs\,ds, \tag{16}$$

where δ_{ls} is the Kronecker delta function, both n_l and n_s the number densities of each sphere, and Q the wave number. The $g(s)$ for bidisperse suspension, which takes three kinds of particle correlations simultaneously, measures the relative density of neighboring spheres at a distance s from a reference sphere. It is known that the Fourier transformation from Q-space (reciprocal space) to real space gives $g(s)$.

4. Results and discussion

4.1. Interaction energy

Fig. 2 shows the electrostatic interaction energy between two dissimilar spheres having an equal dimensionless surface potential of 1. The dimensionless surface charge density corresponding to 3.06 for $a_1 = 20$ nm is estimated as 4.06, 3.06, 2.56, and 2.31, as the a_2 values increase as 10, 20, 40, and 80 nm. The interaction energy increases as the sphere radius ratio $(= a_2/a_1)$ increases. We recognize that, if the radius of one sphere in two charged spheres is constant and the other approaches infinity, the other sphere is similar to a charged flat plate. Our results are compared to the analytical approximate results by employing the leading term of the linear superposition with respect to unperturbed potentials, viz. [10],

$$E_{\mathrm{EL}}^{\mathrm{LSA}}(s') = 4\pi a_l a_s \varepsilon \psi_{s,l}\psi_{s,s}\frac{\exp(-\kappa s')}{s}. \tag{17}$$

It is seen that the analytical approximate results become obviously unreliable as two bodies approach more closely.

Fig. 3 shows that the interaction energy is changed by the variation of solution ionic strength, where the inverse Debye lengths nondimensionalized with sphere 1 $(= \kappa a_1)$ correspond to 0.292, 0.656, 2.06, and 20.6 for solution ionic strengths of 0.02, 0.1, 1.0, and 100 mmol KCl electrolyte concentration. With decreasing solution ionic strength, the interaction energy increases according to the Debye screening effect.

4.2. Radial distribution function

If we treat a monodisperse system with hard spheres, the radial distribution functions g are known analytically in the Percus–Yevick approximation [13,16]. The Metropolis Monte Carlo simulations sample a canonical ensemble

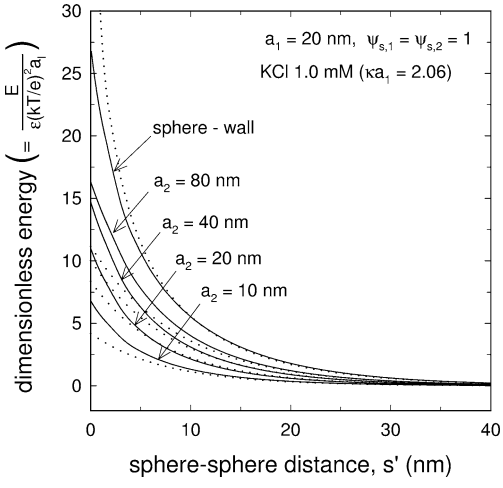

Fig. 2. Dimensionless energy profiles for particle–particle interactions for several particle radius ratios with constant surface-charge boundary conditions and $\kappa a_l = 2.06$, $\kappa a_s = 1.03$. Dotted curves obtained by analytic approximation correspond to each particle radii ratio, from the top.

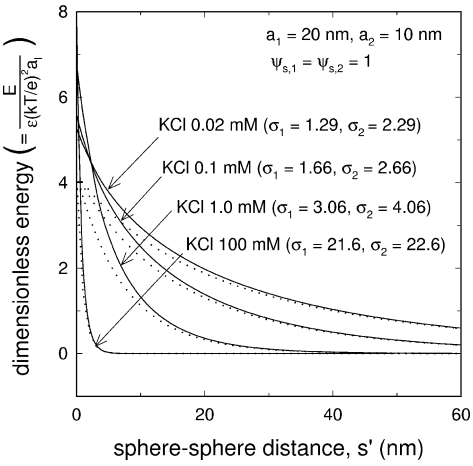

Fig. 3. Dimensionless energy profiles for particle–particle interactions for several inverse Debye lengths with constant surface-charge boundary conditions, $a_l = 20$ nm, and $a_s = 10$ nm. Dotted curves obtained by analytic approximation correspond to each inverse Debye length.

for which the number of particles, temperature, and volume are constant (i.e., NVT). In the NVT process, the probability governing the random particle displacement is justified as $\min[1, \exp(-\Delta E/kT)]$, where $\Delta E = E_{\text{trial}} - E_i$ for the ith step. If the random number is less than this probability, the respective moves are accepted; otherwise the moves are rejected. During the simulations, the total energies after the particle displacements are evaluated using a pairwise additive principle with respect to sphere–sphere interactions. We determine the instantaneous interaction energy at arbitrary sphere–sphere separation distances by interpolating with Newton–Gregory forward polynomials of degree 7. The number of tabulated points for the interpolation ranged from 20 to 28. Interpolating with polynomials was checked by comparing with fitted energy profiles that decay exponentially as functions of the separation distance and the regression coefficients.

In the present study, spheres with a total number of 200–400 are introduced in a simulation box. For the particle displacements, the sizes of the random steps in the three coordinate directions are chosen to be 50% of the corresponding dimension of the periodic unit cell. The total volume fraction C equals the addition of volume fractions for large spheres C_l and small spheres C_s. Discarded nonequilibrium configurations and production configurations are taken to be about 2×10^4 and 4×10^4, respectively. For an initial condition, we use spheres arranged in face-centered cubic lattices. Fig. 4 illustrates the changes of configurations in the periodic unit cell of the cubic box.

We implement a computation of the radial distribution function using a virial expansion based on the integral equation method to compare with Monte Carlo simulation results. The total correlation function $h(r) = g(r) - 1$ is calculable by solving the Ornstein–Zernike equation, given by

$$h(\mathbf{r}) = c(\mathbf{r}) + \sum_i n_i \int n_i c(\mathbf{r}_1) h(\mathbf{r} - \mathbf{r}_1)\, d\mathbf{r}_1. \tag{18}$$

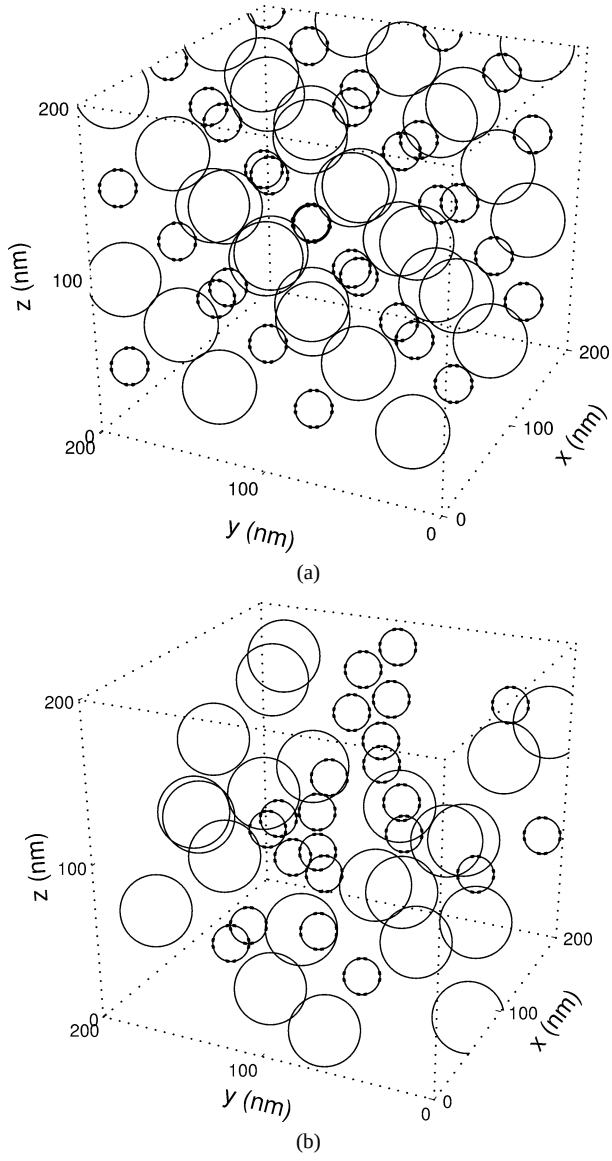

Fig. 4. Snapshots of particle configurations in the simulation box for $a_l = 20$ nm, $a_s = 10$ nm, $\kappa a_l = 2.06$, $\kappa a_s = 1.03$, $C = 0.1$, and $C_l/C_s = 7.38$: (a) initial configurations and (b) 3×10^4 configurations.

Here, $c(\mathbf{r})$ is the direct correlation function and using the Percus–Yevick closure solves Eq. (18). Then we can proceed to the particle concentration profile $C(s)$ with the particle concentration in the bulk C, expressed as

$$g(s) = \frac{C(s)}{C} = \exp\left(-\frac{E(s)}{kT}\right)\left(1 + CY_1(s) + \cdots\right), \tag{19}$$

where the first virial coefficient is defined as

$$\begin{aligned} Y_1(s) &= \int \left[\exp\left(-E(s)/kT\right) - 1\right] f(\mathbf{r}, \mathbf{r}_1)\, d\mathbf{r}_1 \\ &= \int \left[\exp\left(-E(s)/kT\right) - 1\right] \\ &\quad \times \left[\exp\left(-E(\mathbf{r}, \mathbf{r}_1)/kT\right) - 1\right] d\mathbf{r}_1. \end{aligned} \tag{20}$$

In the above equation, one sphere (sphere 1) is at position $\mathbf{r}$, a distance s from a second sphere, and a third sphere is

at position $\mathbf{r}_1$. The integral is over all space around one sphere, and the Mayer function $f(\mathbf{r}, \mathbf{r}_1)$ depends on the sphere–sphere interaction. The Y_1 is defined in terms of

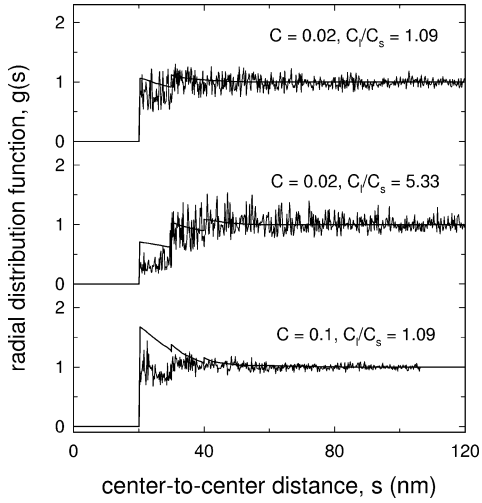

Fig. 5. Comparison of radial distribution functions for uncharged case between Monte Carlo results and virial expansion results.

configuration-space integrals that involve interactions both between sphere 1 and sphere 2 and between sphere 1 and sphere 3. Each individual $g(s)$ is estimated for a total of eight cases, in which three spheres are alternately assigned with possible combinations of large and small ones. Overall $g(s)$ can be obtained by weighting the individual $g(s)$ with corresponding possibility of choosing. In spite of the uncharged particle system, the second virial coefficient for a bidisperse system contains cumbersome integral terms. For the case of a monodisperse system, it is known that only the first-order effect of C can be reasonably considered without great loss of accuracy [17]. In Fig. 5, the radial distribution function from Monte Carlo simulations is compared with corresponding predictions from the virial expansions, and fair agreement between the two methods is shown at the lower particle concentration with the lower C_l/C_s. The disagreement is developed, however, once the particle concentration increases at lower C_l/C_s or the C_l/C_s increases at lower particle concentration.

Fig. 6 shows the radial distribution function $g(s)$ for a bidispserse suspension of hard spheres with different total volume fractions as well as a volume fraction ratio C_l/C_s.

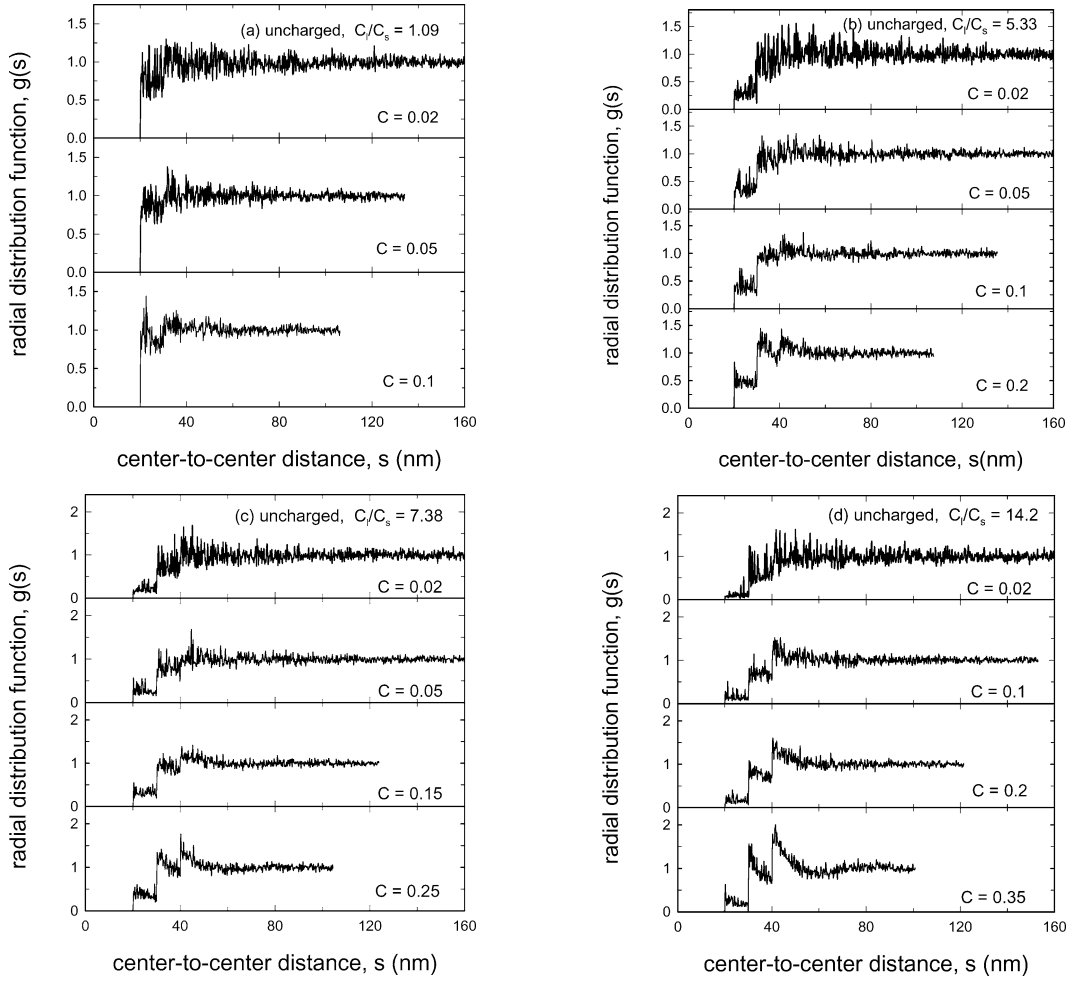

Fig. 6. Comparison of radial distribution functions of uncharged spheres with $a_l = 20$ nm and $a_s = 10$ nm: (a) $C_l/C_s = 1.09$, (b) $C_l/C_s = 5.33$, (c) $C_l/C_s = 7.38$, and (d) $C_l/C_s = 14.2$.

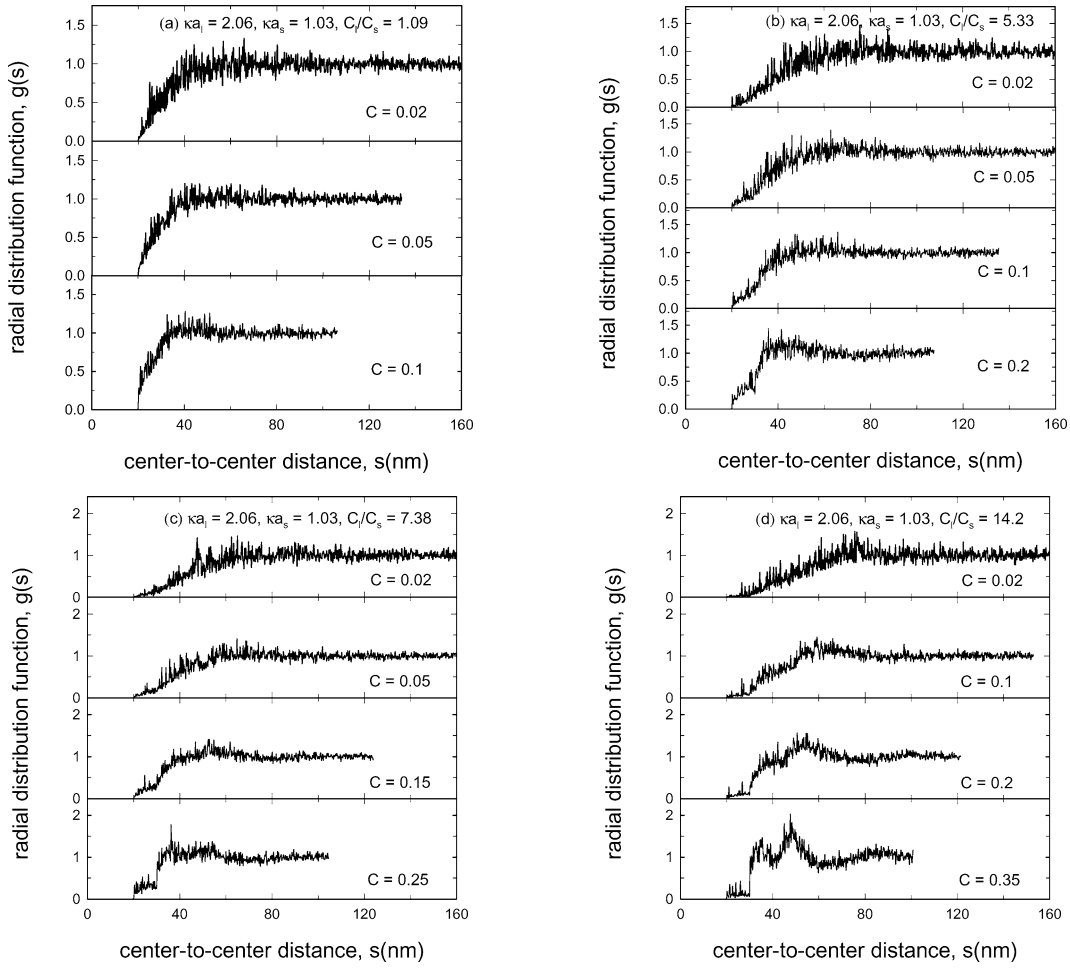

Fig. 7. Comparison of radial distribution functions of charged spheres with $a_l = 20$ nm, $a_s = 10$ nm, $\kappa a_l = 2.06$, and $\kappa a_s = 1.03$: (a) $C_l/C_s = 1.09$, (b) $C_l/C_s = 5.33$, (c) $C_l/C_s = 7.38$, and (d) $C_l/C_s = 14.2$.

The $g(s)$ exhibits damped oscillations with increasing particle concentration, the maxima of which occur near multiples of the nearest-neighbor distance. As the volume fraction ratio increases, the $g(s)$ profile has the splitting shape at the distance positions of 20, 30, and 40 nm for the interactions of small–small, small–large, and large–large spheres. Fig. 7 shows the $g(s)$ for a bidisperse suspension of charged spheres with equal surface potential but different volume fractions. We point out that, compared to the case of uncharged spheres, the repulsive interactions evidently decrease the density near the sphere.

4.3. Osmotic pressure and structure factor

When the particle concentration is zero, the coefficient A_2 has a maximum value corresponding to the dilute limit A_2, and it decreases with increasing particle concentration. Once the values of A_2 are known, both the thermodynamic coefficient and the osmotic pressure can be computed as functions of the particle concentration. Figs. 8 and 9 show that with increasing particle concentration S has an overall decreasing trend, while the osmotic pressure is increased. The volume-

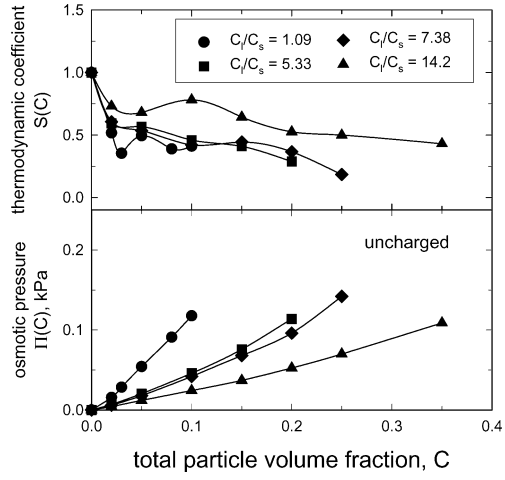

Fig. 8. The plots of the thermodynamic coefficient S and the osmotic pressure Π vs particle concentration with different concentration ratios for uncharged spheres.

average radii of bidisperse spheres are determined as 12.25, 15.61, 16.34, and 17.63 nm with respect to the ratios of particle volume fraction of 1.09, 5.33, 7.38, and 14.2. Regardless

of uncharged or charged cases, as the volume fraction ratio increases, the value of S increases, whereas the osmotic pressure decreases. The charged suspension shows a higher variation of S with increasing particle concentration, which becomes more significant with increasing volume fraction ratio. The increasing tendency of the value of S for particle concentrations above about 0.25 should be noted in the case $C_l/C_s = 14.2$. Evidently, the increase of electrostatic

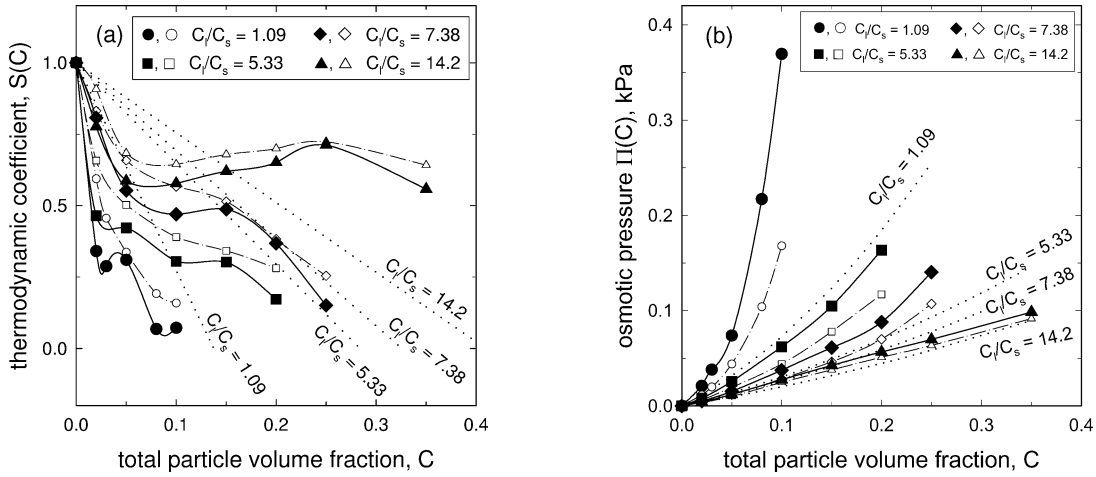

Fig. 9. The plots of (a) thermodynamic coefficient S and (b) osmotic pressure Π vs particle concentration with different concentration ratios for charged spheres with $\kappa a_l = 2.06$ and $\kappa a_s = 1.03$. Open symbols correspond to the Monte Carlo results obtained using the analytical energy profile, and dotted lines are determined using A_2 coefficients for the dilute limit case.

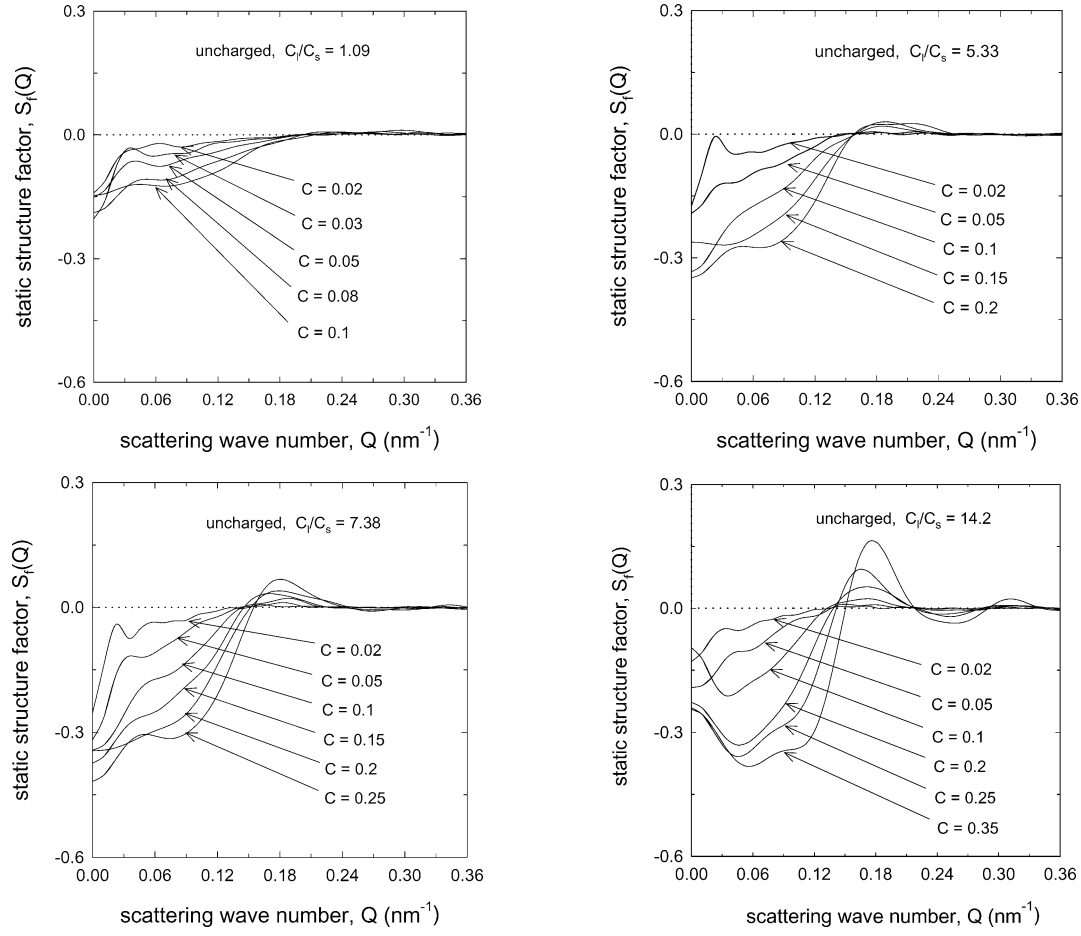

Fig. 10. Comparison of static structure factor $S_f(Q)$ of uncharged spheres for $C_l/C_s = 1.09$, 5.33, 7.38, and 14.2, where $a_l = 20$ nm, $a_s = 10$ nm, and $\lambda = 35$ nm.

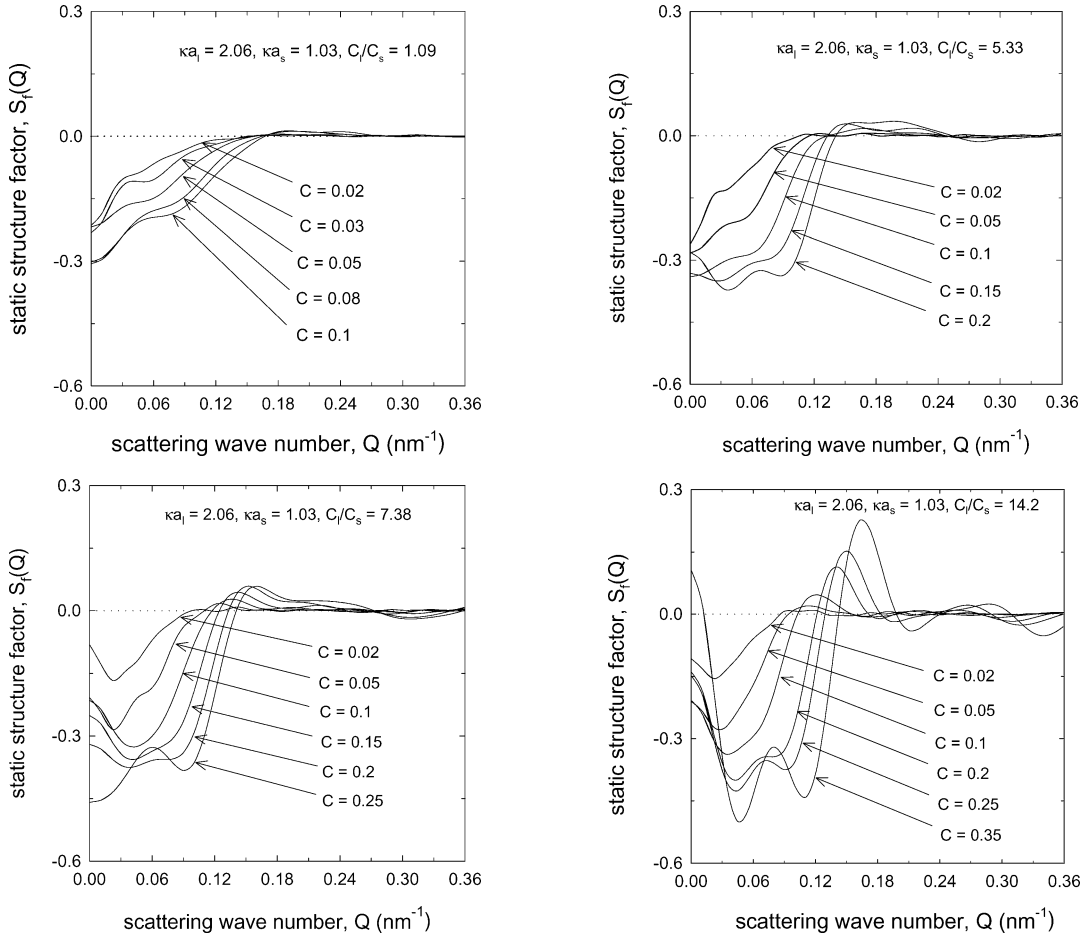

Fig. 11. Comparison of static structure factor $S_f(Q)$ of charged spheres for $C_l/C_s = 1.09$, 5.33, 7.38, and 14.2, where $a_l = 20$ nm, $a_s = 10$ nm, $\kappa a_l = 2.06$, $\kappa a_s = 1.03$, and $\lambda = 35$ nm.

interaction between similarly charged spheres caused by the Debye screening effect provides an increase in the osmotic pressure compared to the uncharged case.

Corresponding results obtained using either the analytic approximation for energy profile or the analytic expression for osmotic pressure are provided in Figs. 9a and 9b, to propose the validity of a rigorous calculation of energy profile as well as Monte Carlo simulations for the radial distribution function. It is evident that the hypothetical results obtained from the dilute limit A_2 show a great deviation. In Fig. 9b, the osmotic pressure obtained using the rigorous energy profile of this study is estimated more than twice that obtained using the analytical energy profile. But the discrepancy between the two results on the volume fraction change is decreased as the composition of the bimodal suspension becomes disparate.

Figs. 10 and 11 indicate that a structure is built up which depends both on the particle volume fraction and the solution ionic strength. The structure factor in this study ensures the total contributions consisting three kinds of particle correlations (i.e., large–large, large–small, small–small). Above all, strong correlations develop between the two different-sized spheres. One would favorably expect that the small spheres would tend to fit into the spaces between the larger ones. This is indicated by the increase in magnitude of the first peak in $S_f(Q)$ and its decrease at low Q values as the volume fraction increases at a given ionic strength. The first peak also moves to higher Q values as the volume fraction increases. Compared between uncharged and charged cases, it can be observed that with an increase in ionic strength at constant volume fraction a broadening of the peak occurs, which indicates a decrease in strength of the interparticle interaction and a greater motion of the spheres.

5. Conclusions

By applying the Monte Carlo simulation, the radial distribution function of the colloidal dispersion with bidisperse spheres was obtained for higher particle concentration up to ca. 30 vol%. Our computations of the energy profile of long-range interaction based on the singularity method provide accurate results for the linearized P–B field.

It is evident that the effect of electrostatic repulsion upon the osmotic pressure due to the Debye screening depends on the particle concentration. As the concentration ratio be-

tween large and small particles decreases, the osmotic pressure is increased at a given total concentration. This trend can be understood from estimating the static structure factor, in which more small particles tending to fit into the spaces between the larger ones results in the increasing the osmotic pressure. The utility of our numerical simulations has been verified by attempting comparison with analytical approximate results.

Acknowledgments

It is a pleasure to acknowledge encouragement from Jae Seol Cho and invaluable help in running the simulation code. This work was supported by the Basic Research Fund (Grant R01-2001-000-00411-0) from the Korea Science and Engineering Foundations (KOSEF) provided to M.-S.C. Also, he thanks the British Council in Seoul for a fellowship, as well as the KOSEF for visiting research 2001.

Appendix A. Nomenclature

a	particle radius (m)
A_2, A_3	osmotic virial coefficients (–)
C	particle volume fraction (–)
c_i^0	concentration of ion species i ($\mathrm{mol/m^3}$)
E	interaction energy (J)
e	elementary electrostatic charge (Coul)
$\mathbf{e}$	unit vector (–)
F	electrostatic force (N)
f	Mayer function (–)
g	radial distribution function (–)
h	total correlation function (–)
$\mathbf{I}$	identity tensor (–)
k	Boltzmann constant (J/K)
M	total number of surface points (–)
N	number of spheres (–)
N_A	Avogadro number (1/mol)
$\mathbf{n}$	unit normal vector pointing into solvent (–)
n	number density ($1/\mathrm{m^3}$)
$\mathbf{Q}$	scattering vector (–)
q	unknown singularity (–)
$\mathbf{r}$	position vector (–)
r	distance normalized by sphere radius (–)
S	thermodynamic coefficient (–)
S_A	surface area ($\mathrm{m^2}$)
S_f	static structure factor (–)
s	center-to-center separation distance (m)
s'	surface-to-surface distance (m)
T	absolute temperature (K)
$\mathbf{T}$	Maxwell stress tensor ($\mathrm{N/m^2}$)
x	Cartesian coordinate (–)
Y_1	first virial coefficient in Eq. (19) ($\mathrm{m^3}$)
Z_i	valence of ion species i (–)

Greek symbols

α	number of off-center singularities (–)
δ	Kronecker delta function (–)
ε	dielectric constant (Coul/V m)
θ	scattering wave angle (deg)
κ	inverse Debye length (1/m)
λ	wavelength in the dispersion medium (m)
$\tilde{\Pi}$	difference in local osmotic pressure ($\mathrm{N/m^2}$)
σ	dimensionless surface charge density (–)
ψ	dimensionless electrostatic potential (–)
ψ_s	dimensionless surface potential of sphere (–)

Subscripts

l	large
s	small

Superscripts

c	center
oc	off-center

References

[1] W.R. Bowen, P.M. Williams, J. Colloid Interface Sci. 184 (1996) 241.
[2] W.R. Bowen, X. Cao, P.M. Williams, Proc. R. Soc. London Ser. A Math. Phys. Eng. Sci. 455 (1999) 2933.
[3] W.R. Bowen, A. Mongruel, P.M. Williams, Chem. Eng. Sci. 51 (1996) 4321.
[4] W.R. Bowen, Y. Liang, P.M. Williams, Chem. Eng. Sci. 55 (2000) 2359.
[5] M.-S. Chun, G.-Y. Chung, J.-J. Kim, J. Membrane Sci. 193 (2001) 97.
[6] R.J. Phillips, J. Colloid Interface Sci. 175 (1995) 386.
[7] T. Dabros, J. Fluid Mech. 156 (1985) 1.
[8] S.L. Carnie, D.Y.C. Chan, J.G. Gunning, Langmuir 10 (1994) 2993.
[9] H. Ohshima, J. Colloid Interface Sci. 162 (1994) 487.
[10] H. Ohshima, J. Colloid Interface Sci. 170 (1995) 432.
[11] S.L. Carnie, D.Y.C. Chan, J. Colloid Interface Sci. 155 (1993) 297.
[12] J.-P. Hsu, B.-T. Liu, J. Colloid Interface Sci. 217 (1999) 219.
[13] W.B. Russel, D.A. Saville, W.R. Schowalter, Colloidal Dispersions, Cambridge Univ. Press, New York, 1989.
[14] R.H. Ottewill, H.J.M. Hanley, A.R. Rennie, G.C. Straty, Langmuir 11 (1995) 3757.
[15] R.H. Ottewill, in: J.M. Asua (Ed.), Polymeric Dispersions: Principles and Applications, in: NATO ASI Series E, Kluwer, Boston, 1996, pp. 229–242.
[16] R.J. Hunter, Foundations of Colloid Science, second ed., Oxford Univ. Press, New York, 2001.
[17] E.D. Glandt, AIChE J. 27 (1981) 51.